International Conference on Adaptive Modeling and Simulation
ADMOS 2005
P. Díez and N.-E. Wiberg (Eds)

HIGH-ORDER H-ADAPTIVE DISCONTINUOUS GALERKIN METHODS FOR OCEAN MODELING

P. E. Bernard[a,b], N. Chevaugeon[c], V. Legat[a,b],
E. Deleersnijder[b,a],J.-F. Remacle[a,c]

[a] Center for Systems Engineering and Applied Mechanics (CESAME),
Université Catholique de Louvain, B-1348 Louvain-la-Neuve, Belgium.

[b] Institut d'Astronomie et de Géophysique G.Lemaître,
Université Catholique de Louvain,B-1348 Louvain-la-Neuve, Belgium.

[c] Département de Génie Civil et Environnemental
Université Catholique de Louvain,B-1348 Louvain-la-Neuve, Belgium.

Key words: Shallow Water Equations, h-Adaptivity, Discontinuous Galerkin.

Summary. *In this paper, we present an h-adaptive Discontinuous Galerkin (DGM) formulation of the shallow water equations. For a DGM scheme using polynomials up to order p, the discretization error of the DGM can be shown to be of the order of h^{p+1}. It can be shown by rigorous error analysis that the DGM discretization error can be related to the amplitude of the inter-element jumps. Therefore we use the information contained in jumps to build error metrics and size field. Some results are presented for ocean modeling problems. A first experiment shows that the theoretical convergence rate is reached with the DGM high-order h-adaptive method applied to the classical Stommel model. A second experiment shows the propagation of an anticyclonic eddy in the realistic domain of the Gulf of Mexico.*

1 Introduction

The Discontinuous Galerkin Method (DGM) has become a very attractive method especially for advection-dominated problems [10, 1, 4]. The main advantage being its flexibility in terms of mesh and shape function while maintaining compactness of the stencil for efficient parallel implementation. Recent advances coming from the integration-free version of the formulation [17, 2], allow to enhance the efficiency of the DGM. The quadrature free implementation is especially useful at high polynomials orders. The DGM has been recently applied to solve shallow-water problem [6, 7]. In our work, we aim to develop circulation model where the geometry, often based on topographic data, is complex enough to justify the shift from traditional ocean modeling cartesian grid model to unstructured meshes[13]. We believe that the DGM is a good candidate for unstructured ocean simulation. In ocean modeling, important dynamics features like eddies have to be followed in time and solved accurately. Dynamic mesh adaptation strategies that follow those structures have great potential in the field of Ocean modeling.

Recent applications [3, 5, 11, 9] show that those technologies are mature enough to tackle difficult problems. The computational overhead of modifying the mesh is insignificant compare to the overall gain in computation time. Starting from a fast implementation of the DGM, originally developed to solve aero-acoustic propagation problem [8], we first discuss the implementation of the shallow-water equations, in particular the choice of a good Riemann solver. After a brief description of the mesh-adaptation package, *MeshAdapt* developed at SCOREC[1] [19, 16], we detail the coupling between the DGM code and *MeshAdapt*. We then provide some preliminary validations of the methods by solving the classical Stommel-Problem, before turning to an idealized simulation of an anticyclonic eddy in the Gulf of Mexico.

2 Discontinuous Galerkin Method for shallow water equations

It's only recently that the DGM has been applied to the shallow water equations (SWEs) [21, 12]. These equations have been used for many years for solving a huge range of problems, such as atmospheric, oceanic, dam breaking or river flow problems [22].

2.1 Shallow water equations

The SWEs describe the flow of a thin layer of incompressible fluid, under the influence of a gravitational force. Those equations are derived from the Navier-Stokes equations by integration over the depth of the fluid layer $H = h+\eta$, where h is the bathymetry and η the relative surface elevation measured from a reference height (figure (1)). The bottom and the surface of the ocean are impermeable, which gives the two boundary conditions required for integration.

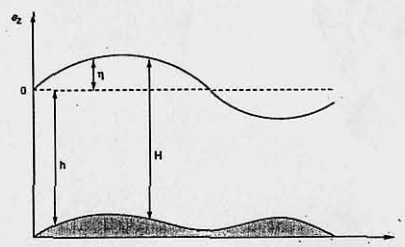

Figure 1: Shallow Water notations for water depth H with a time-independent bathymetry h (Courtesy of Laurent White)

The two-dimensional, inviscid, conservative form of the SWEs reads :

$$\frac{\partial H}{\partial t} + \nabla \cdot (H\mathbf{v}) = 0 \tag{1}$$

$$\frac{\partial H\mathbf{v}}{\partial t} + \nabla \cdot (H\mathbf{v}\mathbf{v}) + gH\nabla\eta + f\mathbf{e}_z \times H\mathbf{v} = -\gamma H\mathbf{v} + \frac{\boldsymbol{\tau}}{\rho} \tag{2}$$

[1] SCOREC, Scientific Computation Research Center, Rensselaer Polytechnic Institute, Troy, NY

where t is time, f is the Coriolis parameter, $\mathbf{v}$ is the depth-averaged velocity, g is the gravitational acceleration, $\gamma H\mathbf{v}$ and $\frac{\tau}{\rho}$ are the bottom and surface stresses, respectively.

Interesting simplifications can be done to the above equations in order to obtain the Stommel model, which possesses an analytical solution. If non linear transport terms can be neglected, with a constant bathymetry and the beta plane approximation in the non conservative form of the SWEs, we obtain the Stommel equations :

$$\frac{\partial \eta}{\partial t} + \nabla \cdot (h\mathbf{v}) = 0 \tag{3}$$

$$\frac{\partial \mathbf{v}}{\partial t} + g\nabla\eta + (f_0 + \beta_0 y)\mathbf{e}_z \times \mathbf{v} = -\gamma\mathbf{v} + \frac{\tau}{h\rho} \tag{4}$$

The free surface allows propagation of gravity waves at speed $c = \sqrt{gH}$, just like the sound waves in acoustic problems. If the water depth is large enough, this involves the resolution of two different phenomenons : the propagation of gravity waves and the movement of the fluid, typically ten to a hundred times slower in ocean applications.

2.2 Discontinuous Galerkin Method applied to SWEs

The difference between the DGM and classical FEMs is that the solution is approximated in each element separately. Two neighboring elements in continuous FEM share a common node, which allows information transfer between them. In DGM, all the nodes lie in their respective element, so that the jumps at interfaces are the only way to generate information transfer across boundaries, by creating fluxes between elements. Jumps clearly contain interesting information, in particular an estimation for the error which will be useful in adaptive developments.

The problem can be expressed as follows without loss of generality. We seek to determine the vector of unknowns $\mathbf{U}(\Omega, t) : \Re^2 \times \Re^2 \rightarrow L^2(\Omega)^m = V(\Omega)$ as the solution of a system of conservation laws :

$$\frac{\partial \mathbf{U}}{\partial t} + \nabla \cdot \mathbf{F}(\mathbf{U}) = \mathbf{S} \tag{5}$$

where $\mathbf{F}$ is the flux matrix and $\mathbf{S}$ is the vector containing the source terms.
In order to obtain a Galerkin form of (5), we can multiply equation (5) by a test function $\mathbf{w} \in V(\Omega)$ and integrate over Ω :

$$< \mathbf{w}\frac{\partial \mathbf{U}}{\partial t} > + < \nabla \cdot \mathbf{F}(\mathbf{U})\mathbf{w} > = < \mathbf{S}\mathbf{w} > \tag{6}$$

with the following operators definitions : $< \cdot >= \int_\Omega \cdot d\Omega$ and $\ll \cdot \gg = \int_{\partial\Omega} \cdot dS$.
The divergence theorem can be used to obtain the following variational formulation :

$$< \mathbf{w}\frac{\partial \mathbf{U}}{\partial t} > - < \mathbf{F}(\mathbf{U}) \cdot \nabla\mathbf{w} > + \ll \mathbf{F}(\mathbf{U}) \cdot \mathbf{n}\mathbf{w} \gg = < \mathbf{S}\mathbf{w} > \tag{7}$$

The simplified Stommel equations lead to the following expressions for $\mathbf{U}$ and $\mathbf{F}$:

$$\mathbf{U} = \begin{bmatrix} \eta \\ u \\ v \end{bmatrix} \qquad \mathbf{F}(\mathbf{U}) = \begin{bmatrix} hu & hv \\ g\eta & 0 \\ 0 & g\eta \end{bmatrix} \tag{8}$$

The discrete solution $\mathbf{U}^h$ is completely discontinuous between elements. Information can thus only propagate through fluxes between adjacent elements. But the values of $\mathbf{U}^h$ at the discontinuities $\partial\Omega$ are not well defined. Those values and the corresponding fluxes can be expressed as the approximate solution of a Riemann problem [15].

The general form equation (5) can be expressed as :

$$\frac{\partial \mathbf{U}}{\partial t} + \mathbf{F}_\mathbf{x}\frac{\partial \mathbf{U}}{\partial x} + \mathbf{F}_\mathbf{y}\frac{\partial \mathbf{U}}{\partial y} = \mathbf{S} \tag{9}$$

The projection of (9) on the normal direction to $\partial\Omega$ leads to :

$$\frac{\partial \mathbf{U}}{\partial t} + \mathbf{J}_\mathbf{n}\frac{\partial \mathbf{U}}{\partial x} = \mathbf{S} \tag{10}$$

where the tangential component has been neglected. The matrix $\mathbf{J}_\mathbf{n}$ can be written as $\mathbf{J}_\mathbf{n} = \mathbf{R}\mathbf{\Lambda}\mathbf{R}^{-1}$ with matrices of eigenvectors $\mathbf{R}$ and eigenvalues $\mathbf{\Lambda}$. Then we obtain the following one-dimensional transport equation :

$$\frac{\partial \mathbf{U}^*}{\partial t} + \mathbf{\Lambda}\frac{\partial \mathbf{U}^*}{\partial x} = \mathbf{R}^{-1}\mathbf{S} \tag{11}$$

The "characteristics" variables $\mathbf{U}^* = \mathbf{R}^{-1}\mathbf{U}$ are convected along the normal direction to the edge of the element. The transport velocities are the eigenvalues of the problem. For the Stommel equations, eigenvalues are given by :

$$\mathbf{\Lambda} = \begin{bmatrix} \sqrt{gh} & 0 & 0 \\ 0 & -\sqrt{gh} & 0 \\ 0 & 0 & 0 \end{bmatrix} \tag{12}$$

Those eigenvalues are used to choose the appropriate values on the edge. More precisely, upwinding can be applied on the "characteristics" variables convected across the edge. It has been shown that this method (the Riemann solver) introduces the minimum numerical dissipations needed to stabilize the numerical scheme in the presence of transport terms.

In order to keep the same general formulation (5), the transport terms require the use of the conservative formulation. Advection terms are thus expressed as a divergence $\nabla \cdot (H\mathbf{v}\mathbf{v})$. This conservative form is non linear, even without transport terms, because of the presence of the elevation term $\nabla\left(\frac{H^2}{2}\right)$. But the transport terms lead to a complex and computationally prohibitive solution of the exact Riemann solver. Approximate Riemann solvers are proved to produce more numerical dissipation than the exact solver, but numerical experience suggests

that this choice does not have a significant impact on the accuracy of the solution, especially when polynomial degree increases. The conservative formulation can thus be solved with, for example, a Roe solver, which consists in the exact solution to a linearized Riemann problem, and is consistent with the discrete entropy condition [20]. The basic idea consists in considering that over a small time step, the characteristics curves propagating information can be replaced by straight lines. This approximation leads to consider as constant the eigenvalues and eigenvectors matrices $\mathbf{\Lambda}$ ans $\mathbf{R}$.

The Roe numerical flux for shallow water equations can be written as :

$$\begin{aligned}\mathbf{F}(\mathbf{U})\cdot\mathbf{n} &= \tfrac{1}{2}\left[\mathbf{F}(\mathbf{U_L})+\mathbf{F}(\mathbf{U_R})\right]\cdot\mathbf{n} \\ &+\tfrac{1}{2}Fr\left[\mathbf{F}(\mathbf{U_L})-\mathbf{F}(\mathbf{U_R})\right]\cdot\mathbf{n}+\tfrac{1}{2}c_A(1-Fr^2)\left[\mathbf{U_L}-\mathbf{U_R}\right]\end{aligned} \tag{13}$$

The first term corresponds to the centered flux, the others are dissipation terms. The $_R$ and $_L$ subscripts denote the values of the field on each of the two sides of the interface between two elements. The average Froude number Fr is defined as :

$$Fr=\frac{\mathbf{v}_A\cdot\mathbf{n}}{c_A} \tag{14}$$

and acts exactly as the Mach number in acoustics problems. This quantity and the average gravity waves speed c_A are based on the Roe's averages, used to linearize the Riemann problem :

$$u_A=\frac{u_L\sqrt{h_L}+u_R\sqrt{h_R}}{\sqrt{h_L}+\sqrt{h_R}} \qquad v_A=\frac{v_L\sqrt{h_L}+v_R\sqrt{h_R}}{\sqrt{h_L}+\sqrt{h_R}} \qquad c_A=\sqrt{g\frac{h_L+h_R}{2}} \tag{15}$$

3 Mesh-adaptation scheme

Mesh-adaptation technic has seen lots of recent development that make it an attractive method to apply in lots of Engineering domain. [19, 3, 5, 11] The *MeshAdapt* software package, perform local mesh modification in order to adapt the mesh to a given metric field. It is able to perform $3D$ anisotropic mesh adaptation in parallel. In this work we only use a subset of this package : since we are interested in solving shallow water problem, only $2D$ mesh adaptation will be used. We will also, for our first experience in coupling ocean modeling and meshadaptation restrain ourself to isotropic mesh adaptation in order to simplify the metric definition. We briefly describe the mesh modification technics detailed in [19, 16, 18] to focus our attention to the definition of the mesh metric

3.1 Description of the mesh adapt package

Given a mesh metric defined over the domain, in our case an isotropic size defined at each node, the mesh adaptation procedure iteratively modifies the local mesh so that the actual size fits the desired size field. The local mesh modification operation used to adapt the 2 dimensional mesh includes entity splitting, edge collapsing and edge swapping operations. The mesh adaptation algorithm consist of :

- identify those mesh entities not satisfying the mesh size.

- perform appropriate mesh modifications so that local mesh will better satisfy the mesh size eld
- repeat above steps until the mesh size is satisfied to an acceptable degree.

To identify mesh entities that need modification, edge length are compared to the size field and marked to be collapsed or splited. Since it is not possible to ensure all mesh edges perfectly match the size field, the transformed length of all mesh edges falls into a small interval close to one. Particularly, we choose interval $[0.5; 1.4]$. The reason for using such an interval is to ensure that the two new edges from a bisection will not be short edges so that oscillation between refinning and coarsening are prevented. A mesh edge is considered short if its transformed length is less than the lower bound of the interval and a mesh edge is considered long if its transformed length is greater than the upper bound. Flat triangles may still exist after mesh modifications : all the edges may satisfy the criteria but the element is poorly shaped. A criteria is therefore used to detect those elements which are eliminated by a combination of edge swap and collapse. More details about the mesh adaptation technics used can be found in [19, 16, 18]

3.2 Defining the mesh size field

In order to define a mesh size field, we have to somehow link an error estimation to the desired size field. While super-convergence has been shown for the eigen values of the convective operator of the DGM scheme, point wise error is known to be of the order of h^{p+1}. Superconvergence also exists at the downwind side of interface between elements for convective variables [1], if the solution is smooth. This superconvergence allows to demonstrate that the jump between elements of any variable constitutes an error estimator : the jump between elements converges at the same rate as the size. For each interelement interface i, we first compute the integral of the jump J_i, over the interface, of one chosen monitor variable : $J_i=\int_i U_L-U_R ds$. In the case of shallow water equation, we always peak the elevation η. Then, for each topological node of the mesh, we define the error estimator as the maximum of the J_i for each edge (in $2D$), or face for 3D cases, connected to this node. This define E_n, the error estimator for the patch of elements connected to the node n. We then need to compute the targeted edge size around each node. The user defines a target error, E_t : the desired maximum of E_n around each node. Results from error analysis previously cited leads us to estimate : $E_t=C_n h_{tn}^{p+1}$, $E_n=C_n h_n^{p+1}$, where C_n is an unknown constant dependent on the shape of the patch around node n, and h_n an actual characteristic length of the elements around node n and h_{tn} the one that should lead to the targeted error. In our case, we defined h_n as the mean length of edge connected to node n. For each node, the target length is computed as :

$$h_{tn}=h_n\left(\frac{E_t}{E_n}\right)^{\frac{1}{p+1}} \tag{16}$$

The target length as computed is valid for any order of p and does not rely on the computation of the gradient or Hessian of the solution field. The size field is then sent along with the mesh to the mesh-adapt package which applies the previous algorithm to adapt the mesh.

3.3 Projection of the solution

Once the mesh has been adapted the solution on the old mesh has to be projected from the old mesh to the adapted one. This is done by means of an L_2 projection. In case of the DGM, this projection is quite cheap, since it can be done element per element. Some diffusion error due to the projection can be expected where swapping operation is applied. In practice, only a small amount of diffusion appears, since swap only occurs to remove bad shaped element. This would not be the case if we had allowed node repositioning as a valid mesh modification procedure. Dispersive error is also only linked to the swap operation, but is only due to the precision of the integration scheme for the L_2 projection, and is therefore controlable. Where ever extra precision is needed, no projection error exists since only edge splitting appends. Projection after a collapse also create some error, but collapse only happens when the error is under the target.

4 Application to Ocean modeling

In this section, we first perform a convergence experiment with an adaptive strategy, in order to test both the convergent behavior of the DGM scheme and the efficiency of the adaptive strategy. In a second experiment, we simulate the propagation of a typical anticyclonic eddy in the realistic domain of the Gulf of Mexico.

4.1 Adaptive convergence applied to the Stommel equations

The following convergence study is performed using the Stommel Problem : the Stommel equations are solved on a one thousand kilometers square, and compared to the analytical solution. The Coriolis effect leads to a geostrophic balance, creating a recirculation cell. The linear part βy of the Coriolis factor f tends to move the created balance westward (for the northern hemisphere parameters), leading to a boundary layer. The adaptive method is therefore very useful in order to capture the large gradients on this western boundary, while the eastern part of the domain don't require such a fine discratization.
Two different polynomial order (P1 and P4) have been used, giving two different theorical convergence rates, according h^{p+1}.

The figure (2.a) presents the evolution of the L_2 error norm with the characteristic element size on a regular mesh. The numerical results show a classical asymptotic behaviour. The figure (2.b) presents the evolution of the L_2 error norm with the size of the elements corresponding to a given target error (equation (16)). The numerical results are compared to the theorical convergence rates lines.
Numerical results fit the theorical rates, both with fixed regular mesh and adapted mesh. Akind of oscillatory behaviour is still present on the adaptive mesh which can be explained with the use of the interval $[0.5; 1.4]$ to transform the error estimation into a new edge size field, as discussed in the previous paragraph.
To reach the same error norm of approximatly $5\ 10^{-3}$ with linear shape functions, the non-adaptive structured regular mesh requiered 648 elements while the adaptive method needs only 79 elements.

On the same mesh, the error is more than a hundred times smaller with $P4$ element than

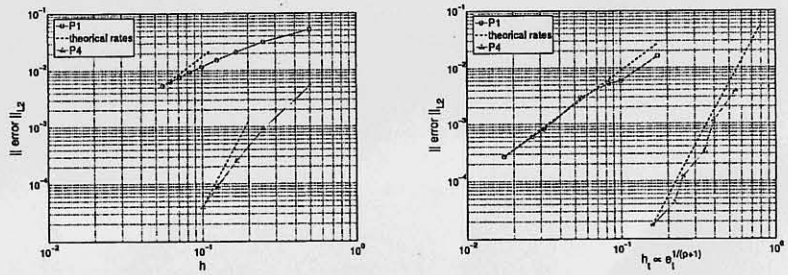

(a) structured mesh (b) adaptive mesh

Figure 2: Convergence of the L_2 error norm with the decreasing characteristic element size h on structured mesh and h_t (the element size corresponding to a given target error e_t according to $h_t \propto e_t^{\frac{1}{p+1}}$) on adaptive mesh.

with $P1$. Our choice of mesh size field based on the only interface element jump leads to the right convergence rate, regardless of polynomial order.

4.2 Propagation of anticyclonic eddy at midlatitudes

The following result consists in the propagation of a typical anticyclonic eddy at midlatitudes. The Gulf of Mexico is chosen as the domain to test the model in a realistic geometry. The basin is assumed closed, the Yucatan Channel and the Florida Straits with their inflow and outflow are ignored. Altough this experiment is highly idealized, it is expected to represent some of the features of the life cycle of anticyclonic eddies with the adaptive capture of eddies propagation. A Gaussian distribution of water elevation η is present at initial time, with an initial velocity field taken to be in geostrophic balance, which means :

$$g' \nabla H = f \mathbf{e}_z \times \mathbf{v} \tag{17}$$

where the β-plane assumption is made (i.e. $f = f_0 + \beta y$) and with g' the reduced gravity. No wind forcing and no bottom friction is applied. The Coriolis effect is thus the only source term to move the eddy westward. This propagation of slow Rossby waves, represented with the SWEs, has a major effect on the large scale circulation, and thus on weather and climate. For instance, Rossby waves can intensify western boundary currents, which transport huge quantities of heat. Even a minor shift in the position of the current can thus dramatically affect weather over large areas of the globe.

Figure (3) represents the evolution of the eddy with the Coriolis forcing. Its westward propagation is captured by the mesh evolution (right column) : a minimum edge size of ten kilometers has been applied to keep a low number of elements.
After one week of physical time simulation, the mesh has been adapted three times to capture

the regions with larger variations : the eddy region, and the coast lines, where gravity waves come and bounce back. At this time, the mesh presents approximately 3000 elements. The eddy keeps moving westward until approximately week 11, when it reaches the coast. Then, its shape is modified when a second eddy appears, spinning in the other direction. The number of elements grows until about 7000 to fit this large variation region. On week 14, one can see the slow creation of a western boundary current, flowing southward. As the eddy keeps moving southward, the mesh seems to perfectly capture the evolution of this current and the swirl generated at the south extremity of the golf on week 23. The initial eddy then collapses to generate lots of smaller eddies which keep spinning and mixing on the western boundary. The number of elements decreases then to the initial value of 3000.
The mesh adapted to eddies and currents, but large field variations and mesh refinement must also be noticed on sharp and non regular coasts, as on the north and east-north of the Gulf.
A restriction of ten kilometers has been applied on the size of elements on adaptive mesh. To reach the same accuracy with a non-adaptive mesh, about 34000 elements would be required with the first order polynomial shape function.

5 Conclusion

In this paper we have shown that mesh adaptivity, coupled with discontinuous Galerkin method, can be a very attractive technology for the ocean modeling field. Of course, in terms of the physic that need to be modeled lots of work need to be done in code implementation in order to compare with established ocean model. Our next step toward this goal will be the ability to deal with realistic bathymetry. On the mesh adaptation side of the work, we plan to take full advantage of the anisotropic mesh adaptation feature of the *MeshAdapt* package.

Acknowledgements

Eric Deleersnijder is a Research associate with the Belgian National Fund for Scientific Research (FNRS). The present study was carried out within the scope of the project "A second-generation model of the ocean system", which is funded by the *Communauté Française de Belgique*, as *Actions de Recherche Concertées*, under contract ARC 04/09-316. This work is a contribution of SLIM, the Second-Generation Louvain-la-Neuve Ice-ocean Model. The authors gratefully acknowledge Emmanuel Hanert for the comments and help he provided during the preparation of this paper.

REFERENCES

[1] S. Adjerid, K.D. Devine, J.E. Flaherty, and L. Krivodonova. A posteriori error estimation for discontinuous Galerkin solutions of hyperbolic problems. *Computer Methods in Applied Mechanics and Engineering*, Vol. 191, 1097–1112, (2002).

[2] H.L. Atkins and C.W. Shu. Quadrature-free implementation of discontinuous galerkin methods for hypebolic equations. *AIAA Journal*, Vol. 36.5, (1998).

[3] T.J. Baker. Mesh adaptation strategies for problems in fluid dynamics. *Finite Elem. Anal. Des.*, Vol. 25(3-4), 243–273, (1997).

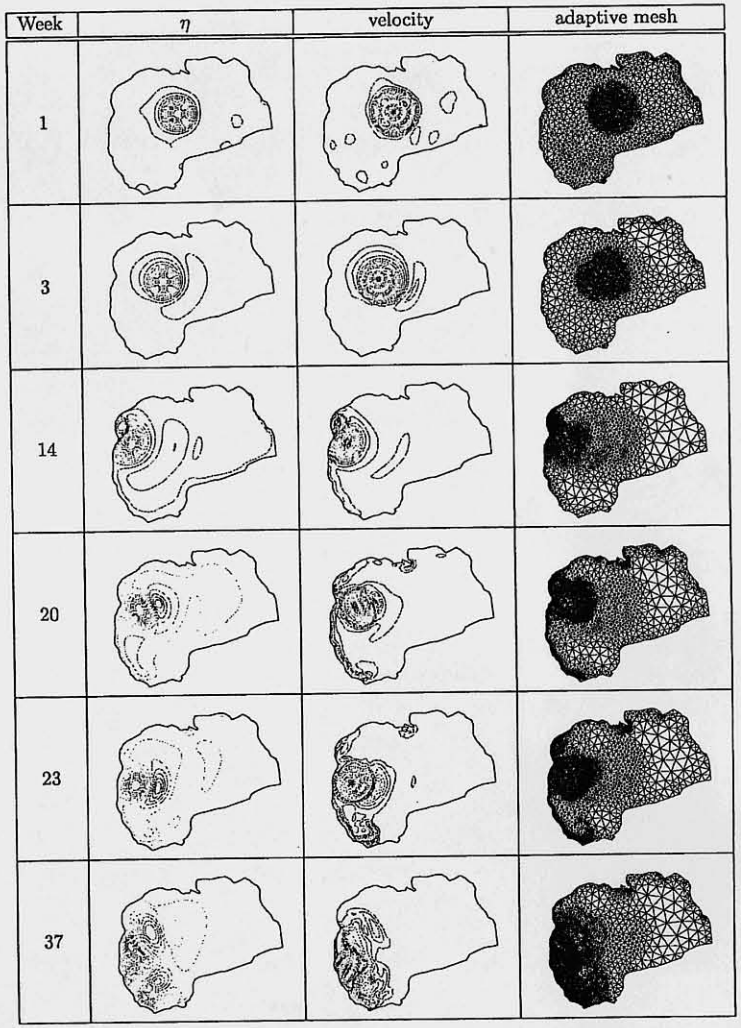

Figure 3: Isolines of elevation field and velocity norm, and the corresponding adaptive mesh, respectively, at different times of the eddy propagation.

[4] F. Bassi and S. Rebay. A high-order accurate discontinuous finite element solution of the 2d Euler equations. *Journal of Computational Physics*, Vol. 138, 251–285, (1997).

[5] M. Berzins and W. Speares. A 3d unstructured mesh adaptation algorithm for the time-dependent shock-dominated problems. *International Journal for Numerical Methods in Fluids*, Vol. 25(1), 81–104, (1997).

[6] C. Dawson and J. Proft. Discontinuous and coupled continuous/discontinuous galerkin methods for the shallow water equations. *Computer Methods in Applied Mechanics and Engineering*, Vol. 191(41-42), 4721–4746, (2002).

[7] C. Dawson and J. Proft Coupled discontinuous and continuous galerkin finite element methods for the depth-integrated shallow water equations. *Computer Methods in Applied Mechanics and Engineering*, Vol. 193(3-5), (2004).

[8] N. Chevaugeon, J. Remacle, Gallez, P. Ploumans, and S. Caro. Efficient discontinuous galerkin methods for solving acoustic problems. *11th AIAA/CEAS Aeroacoustics Conference*, 2005.

[9] N. Chevaugeon, J. Xin, P. Hu, X. Li, D. Cler, and J.E. Flaherty and Mark S. Shephard. Discontinuous galerkin methods applied to shock and blast problems. *Journal Scientific Computing*, 22(1), 227–243, (2005).

[10] B. Cockburn, G.E. Karniadakis, and C.W. Shu. *Discontinuous Galerkin Methods*. Lecture Notes in Computational Science and Engineering. Springer Verlag, (2000).

[11] P.L. George, H. Borouchaki, and P. Laug. An efficient algorithm for 3d adaptive meshing. *Advances in Engineering Software*, 33(7-10), 377–387, (2002).

[12] F. Giraldo, J. Hestheaven and T. Wartburton, Nodal high-order discontinuous galerkin methods for the spherical shallow water equations. *Journal of Computational Physics*, Vol. 181, 499–525, (2002).

[13] E. Hanert, D. Y. Le Roux, V. Legat, E. Deleersnijder, Advection schemes for unstructured grid ocean modelling. *Ocean Modelling*, Vol. 7, 39–58. (2004).

[14] E. Hanert, D. Y. Le Roux, V. Legat, E. Deleersnijder, An efficient finite element method for the shallow water equations. *Ocean Modelling*, Vol. 10, 115–136. (2005).

[15] R. LeVeque, *Numerical Methods for Conservation Laws*, Birkhuser-Verlag, (1992).

[16] X. Li. *Mesh Modification procedure for General 3-D Non-Manifold Domaines*. PhD thesis, Renselear Polytechnic Indtitute, (2003).

[17] D.P. Lockard and H.L. Atkins. Efficient implementations of the quadrature-free discontinuous galerkin method. *Proceeding of 14th AIAA CFD conference*. AIAA, (1999).

[18] X. Li, J-F. Remacle, N. Chevaugeon, .M. Shephard Anisotropic Mesh Gradation Control *13th Internationnal Meshing Roundtable*. (2005).

[19] J.F. Remacle, X. Li, M.S. Shephard, and J.E. Flaherty. Anisotropic adaptive simulation of transient flows using discontinuous galerkin methods. *International Journal for Numerical Methods in Engineering*, Vol. 62(7),899–923, (2005).

[20] P. L. Roe, Approximate Riemann Solvers, parameter vectors and difference schemes. *Journal of Computational Physics*, Vol. 43, 357–372, (1981).

[21] D. Schwanenberg and J. Kongeter, A discontinuous Galerkin method for the shallow water equations with source terms. *Discontinuous Galerkin Methods, volume 11 of Lectures Notes in Computational Science and Engineering*, Berlin, 419–424, (2000).

[22] C.B. Vreugdenhill. *Numerical Methods for Shallow Water Flow*, Water Science and Technologie Library, Kluwer Academic Publishers, (1994).